Coherent quasielastic Bragg scattering from single crystals containing fast diffusers

K. Ruebenbauer* and U. D. Wdowik
Institute of Physics and Computer Science, Pedagogical University, PL-30-084 Cracow, ul. Podchorążych 2, Poland
(Received 21 January 1998)

Recent developments in the nuclear resonant (Mössbauer) scattering of synchrotron radiation (NRSR) allowed one to observe successfully diffusive quasielastically scattered radiation from intermediate nonresonant amorphous targets, e.g., glycerin, in a time domain. Hence, there is a real chance to observe such a radiation scattered coherently at Bragg angles from single crystals containing fast diffusing atoms. Quasielasticity of the latter radiation is solely caused by jumps between various Bravais lattices due to the peculiarity of the Bragg conditions. On the other hand, an energy resolution could be easily increased by two orders of magnitude in comparison with the incoherent quasielastic scattering of the cold neutrons (QNS) at much higher momentum transfer to the crystal than in the case of QNS. The paper is devoted to a discussion of the physics underlying scattering of NRSR beams from fast diffusers in single crystals under Bragg conditions.
[S0163-1829(98)07741-8]

I. INTRODUCTION

A recent development in the nuclear resonant scattering of synchrotron radiation (NRSR) allows one to investigate quasielastic processes in nonresonant targets in the neV resolution range typical for a ^{57}Fe Mössbauer spectroscopy, where the wave number of the incident radiation is about 7.3 $Å^{-1}$.[1] Previously such experiments were limited to the tungsten Mössbauer line,[2] where sufficiently strong sources could be obtained. An energy resolution of the latter line is of the order of 1 μeV, i.e., comparable to the resolution of the best back-scattering cold neutron spectrometers,[3] albeit offering a much broader momentum transfer range. An energy profile of the nonresonant quasielastic scattering of the ^{57}Fe 14.4 keV line from single crystals was seldom observed due to the unavailability of sufficiently strong, and simultaneously resonantly thin, sources.[4] Amorphous targets were investigated by the latter method due to the much less demanding geometry.[5] One has to note that high-energy resolution neutron spectrometers are available, but at very small momentum transfers solely.[6] Hence, slow diffusivity studies were practically limited to iron as far as microscopic methods sensitive to the wave-vector transfer are considered.[7]

NRSR investigations are conveniently carried out in a time domain,[8] and it has been demonstrated that a resonant forward scattering is sensitive to diffusive motions of resonant scattering atoms in complete agreement with the standard absorption or emission Mössbauer spectroscopy.[9] One can speculate that the same statement applies to resonant Bragg scattering and resonant incoherent scattering as well.[10]

Recently a device shown in Fig. 1 has been built and used to demonstrate the presence of diffusive quasielastic scattering from an amorphous target, i.e., glycerin,[11] the latter system being quite well understood[12] due to previous research performed either by using a standard absorption Mössbauer spectroscopy on doped samples[13] or scattering of the tungsten line from the pure samples at higher temperatures.[14] An iron line was used in a scattering experiment performed on the above system as well.[5]

The above-mentioned device could be used as well to look upon diffusivity in single-crystals scattering at Bragg angles and do not contain resonant nuclei, i.e., for a scattering via the Rayleigh mechanism. A setup is quite similar to the standard four-circle x-ray diffractometer; however, a new dimension (time-energy) is added. In principle, powder samples could be used as well, however at the cost of an enormous loss in intensity. One has to note that in the case of naturally very-well-collimated NRSR beams a single-crystal experiment is in principle much easier than one performed on an amorphous system. The situation is the opposite for radioactive sources emitting radiation spherically.

The paper is organized as follows: Section II deals with a brief description of the essential features of the device shown in Fig. 1 and Sec. III is devoted to the description of the quasielastic scattering function under Bragg conditions, while a simple example is evaluated in detail in Sec. IV. Section V is devoted to a discussion of correlated jumps and the final Sec. VI summarizes results.

II. NRSR INTERFEROMETER

A NRSR interferometer has been introduced quite recently and used to study diffusivity in glycerin.[11] Basic features of the above device are shown in Fig. 1. A pulsed beam of x rays comes at regular time intervals from an undulator with the first harmonic tuned to the Mössbauer transition. Such a beam consists of very-short-duration and very intense pulses, and it has a very small overall cross section and divergence. It is linearly polarized to a high degree as well. The beam is monochromatized to several meV by a set of single-crystal monochromators (not shown). It remains still ''white'' and short pulsed from the point of view of the Mössbauer nucleus after such a monochromatization. A monochromatization preserves polarization as well. Subsequently, the beam is passed through a single line flat and homogeneous Mössbauer absorber moving with a constant velocity along the beam (the velocity is very small compared to the velocity of light in vacuum). The part of beam which was not absorbed goes through a collimator and scatters from a single-crystalline target set under Bragg conditions on a head of a four-circle goniometer. It is important to set a

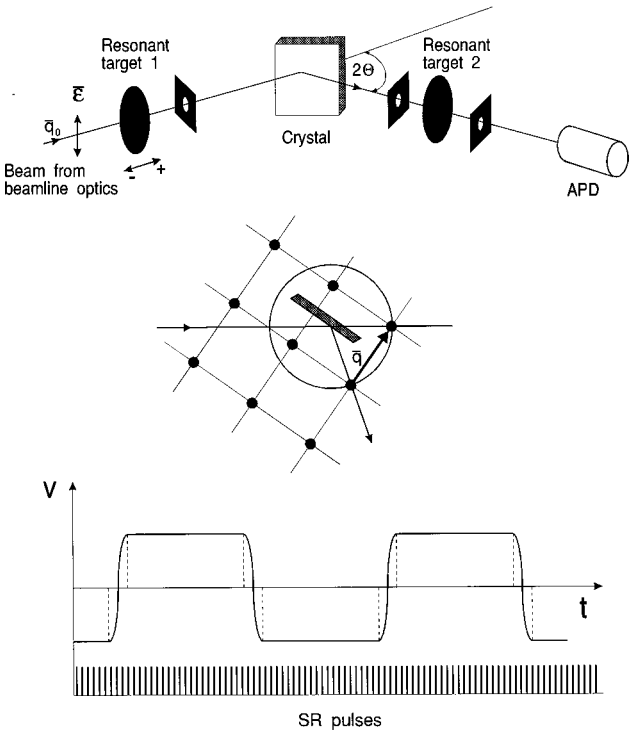

FIG. 1. A general layout of the NRSR interferometer applied to study diffusivity in single crystals under Bragg conditions. Insets show an Ewald construction for the Bragg conditions with the reciprocal lattice cross section overlaid and the velocity of the Doppler modulator vs time with the train of the undulator pulses (the time scale of the pulse train is expanded in comparison to the modulator scale).

crystal in such a way to allow for a single Bragg reflection to be present in order to avoid a loss in intensity. It seems impractical to use forward scattering as the latter beam is contaminated by the noninteracting part. A backward geometry allows one to use thick crystals, and hence, it seems the most suitable. One has to note that in the region of fast diffusivity a kinematic approximation to the scattering is quite satisfactory. A crystal mosaicity might be a problem for almost perfect beams coming down the undulator, and thus it might be desirable to use single-crystal monochromators, being able to increase somewhat the beam divergence (such a beam would be still perfectly collimated from the Mössbauer point of view). A scattered beam is passed again through the collimator and a stationary Mössbauer absorber identical with the movable one and kept under the same thermodynamical conditions. Identity of both absorbers assures the deepest possible modulation. Finally, the beam goes through the final collimator and falls onto an avalanche photodiode detector (APD). Two last collimators together with a stationary absorber and APD are to be mounted on a movable arm of the four-circle goniometer, being actually a goniometer of the four-circle x-ray diffractometer. Delayed coherently forward scattered photons from the movable absorber pass the same optical path as the original pulse (the nonresonant Bragg scattering cross section is practically the same for all photons within the beam) and they interfere with the delayed coherently forward scattered photons from a stationary absorber. There is no phase shift just after the pulse due to the identity of optical paths. Remaining delayed photons cannot reach the APD for a geometry chosen. For a time duration between subsequent pulses being long enough to get rid of delayed photons and a sufficiently narrow geometry there is practically no background, and one can almost neglect all incoherent contributions provided a thermal diffusive scattering (TDS) under Bragg reflection is negligible. An APD signal (count rate versus time elapsed from the pulse) is modulated by a first-order Doppler shift introduced by the first target. Such a modulation makes it much easier to see any quasielasticity in the Bragg scattering and a Doppler modulation is easiest to set to the required frequency, the latter being constrained by the APD time resolution and time interval between pulses. In principle, one can make movable either first or second target or even a crystal (the latter along the wave-vector transfer direction[15]), but it is technically easiest to move the first target. A movable target has to perform of course the periodic motion shown in Fig. 1, and the data collection should be interrupted at the ''turning points'' indicated by the broken lines. One has to note that the cycle period of the target is much longer than the time duration between pulses. Data could not be collected as well for a short time just after the pulse as one has to allow the APD to recover from the prompt, and the data collection has to be stopped just before the next pulse. Usually, an APD count rate is much smaller than the undulator pulse frequency, and hence, one can allow the collection of a single data point at a well-defined time for each undulator period. The processing of such a data point has to be completed prior to the next pulse. An integer number of pulses has to be processed for each ''half'' of the Doppler modulator period (the same for both ''halves''), and an integer number of the full Doppler modulator cycles has to be performed during the data collection.

Due to the fact that Bragg scattering for available x-ray energies is predominantly of the *E1* character, the maximum scattering intensity could be obtained for the polarization plane being perpendicular to the scattering plane (see Fig. 1). This effect would be particularly strong for Bragg reflections scattering at right angles to the original beam, i.e., for a scattering angle 2Θ being close to $\pi/2$. A refraction within a scattering crystal could be neglected in the first approximation.

An APD count rate (number of counts accumulated for a given number of undulator pulses) versus time t elapsed from the pulse is given by the expression (normalized to unity for $t=0$ after having subtracted background, the latter being very small and practically time independent for a well-designed system):[16]

$$I(t)=(L_0\gamma t)^{-1}\exp(-\gamma t)J_1^2((2L_0\gamma t)^{1/2}) \times\{(1+b)+(1-b)[\mathrm{Re}[S(t)]\cos(2\omega_0 t) +\mathrm{Im}[S(t)]\sin(2\omega_0 t)]\}, \quad (1)$$

where L_0 stands for a dimensionless resonant thickness of both targets together (each target has thickness $L_0/2$), γ stands for a natural linewidth of the Mössbauer transition (it is assumed that targets have no intrinsic broadening), J_1 denotes a Bessel function of the first kind and order, and $\omega_0 = v q_0$ with q_0 being to a good approximation a wave number of the Mössbauer line and v a Doppler velocity (positive

for a motion down the beam and negative vice versa). A symbol $S(t)$ stands here for a scattering function from the crystal under investigation. For a purely elastic scattering, $S(t)\equiv 1$. For a time window accessible one can expect $S(0)=1$ and $S(t)$ evolving with time to smaller values due to the diffusive motions. Such an evolution has a monotonic character, while caused by diffusive motions. An imaginary part of the scattering function, $\mathrm{Im}[S(t)]\equiv 0$, for a time window accessible and a temperature range where a thermally driven diffusivity becomes visible (one can neglect quantum diffusivity as very light atoms scatter too weakly to be observable). Thus, the direction of motion of the movable absorber has no effect on the data. For amorphous materials $S(t)$ evolves to zero with time passing, while for the coherent Bragg scattering from crystals it usually evolves to some constant value smaller than unity, albeit greater than zero. If jumps occur solely within Bravais lattices, $S(t)$ remains unity at all times. A parameter $0\leqslant b\leqslant 1$ accounts for all incoherences other than those due to a diffusivity, the latter incoherences being mainly caused by a single-phonon TDS contribution under Bragg reflection, and hence, time independent on the time scale accessible. For a TDS being absent and a perfect device b approaches zero.

Finally, one can conclude this section saying that an APD is going to register any significant intensity for allowed Bragg reflections. Otherwise, the total intensity registered by an APD would be almost negligible for a well-designed geometry; i.e., an incoherent (quasielastic) scattering of the x rays is very weak from single crystals, and one would have to set a very large solid angle to register any significant intensity. One has to note that inelastic (incoherent) scattering (primarily Compton scattering) does not produce collimated patterns as well. Hence, the only significant contamination might come from TDS scattering under Bragg reflection (usually, one can find reflections with a small TDS contribution), and hence, a spectrometric discrimination of the pulses coming from the APD might be quite crude.

III. SCATTERING FUNCTION UNDER BRAGG CONDITIONS

For a purely elastic coherent scattering in the Bragg direction a cross section from the chemical unit cell could be calculated using a standard crystallographic approach in the case of a sample which does not contain resonant nuclei.

Here, one has to take into account an extra dimension, i.e., a time-energy axis. It is a well-known fact that diffusional broadening disappears at Bragg directions on the Ewald sphere for jumps within a Bravais lattice.[17] Hence, one can expect to see solely jumps between various Bravais lattices for a coherent Bragg scattering investigated here.

Thus, it is necessary to consider a diffusion matrix,[18] and a chemical unit cell as an entity having each vertex belonging to a separate primitive Bravais lattice. A diffusion matrix elements could be expressed as follows under such circumstances:

$$W_{ss'}^{(mm')}=\delta_{mm'}\Omega_{ss'}^{(m)}\alpha_{ss'}^{(m)}(\overline{q})$$

and

$$W_{s's}^{(mm')}=\delta_{mm'}\Omega_{s's}^{(m)}[\alpha_{ss'}^{(m)}(\overline{q})]^{\star}\ \text{for}\ s'\neq s,$$

while

$$W_{ss}^{(mm')}=-\delta_{mm'}\sum_{s'\neq s}\Omega_{ss'}^{(m)}\ \text{for}\ s'=s. \tag{2}$$

Here, index m enumerates different kinds of atoms constituting a crystal, while the index s enumerates different primitive Bravais lattices involved. A diffusion matrix is diagonal in the m indices as diffusivity does not transform atoms one into another. Diagonal elements describe an inverse residence time for the mth atom at the sth lattice (with a negative sign), while the off-diagonal elements contain an average jump frequency of the mth atom from the sth to the s'th lattice multiplied by a geometrical factor dependent upon the wave-vector transfer to the crystal $\overline{q}$. A geometrical factor could be expressed as follows:[19]

$$\alpha_{ss'}^{(m)}(\overline{q})=\sum_{n}\rho_{ss'}^{(mn)}\exp(i\overline{q}\cdot[\overline{R}_{s'}^{(n)}-\overline{R}_{s}]),$$

with

$$\sum_{n}\rho_{ss'}^{(mn)}=1\ \text{and}\ \rho_{ss'}^{(mn)}\geqslant 0, \tag{3}$$

where the index n enumerates different sites (vortices) of the lattice s' as seen from any site of the lattice s, $\overline{R}_{s'}^{(n)}-\overline{R}_{s}$ stands for a jump vector from any site of the sth lattice to the nth site of the s'th lattice (relative to a given site of the sth lattice), and $\rho_{ss'}^{(mn)}$ is a relative probability for the above jump. Due to the fact that all sites of the given lattice are equivalent, the following relationship holds: $\alpha_{s's}^{(m)}(\overline{q})=[\alpha_{ss'}^{(m)}(\overline{q})]^{\star}$. Usually, far away jumps do not occur, and hence, the index n has a very limited range for any pair of lattices. One has to note that for $\overline{q}$ being one of the reciprocal lattice vectors (Bragg conditions) all phase factors in the geometrical factor reduce to the nearest neighbor phase factors; i.e., there are no more than eight different such phase factors for the lowest possible symmetry in a three-dimensional space.

For the setup described above one can assume that the scatterer remains at least locally at thermal equilibrium (in fact, a sample has to reach an equilibrium prior to data accumulation). Therefore, the following relationship holds:

$$p_{ms}\Omega_{ss'}^{(m)}=p_{ms'}\Omega_{s's}^{(m)}\ \text{for}\ s'\neq s, \tag{4}$$

where p_{ms} stands for a probability to find atom m in the vertex of the lattice s. Due to the fact that lattices considered are primitive, the above probabilities satisfy the expressions

$$0\leqslant p_{ms}\leqslant 1\quad\text{and}\quad 0\leqslant\sum_{m}p_{ms}\leqslant 1. \tag{5}$$

A frequency $\Omega_{ss'}^{(m)}$ obeys the following relationship at equilibrium:

$$\Omega_{ss'}^{(m)}=[p_{ms}p_{ms'}\omega_{ss'}^{(m)}\omega_{s's}^{(m)}]^{1/2}\ \text{for}\ s'<s, \tag{6}$$

while the corresponding frequency $\Omega_{s's}^{(m)}$ could be obtained from expression (4). Here, frequencies $\omega_{ss'}^{(m)}$ and $\omega_{s's}^{(m)}$ denote jump frequencies of the mth atom from any site of the sth lattice already occupied by the above atom to any site of the s'th lattice, and vice versa. These frequencies satisfy expression (4) as well, i.e., $p_{ms}\omega_{ss'}^{(m)}=p_{ms'}\omega_{s's}^{(m)}$. A frequency $\omega_{ss'}^{(m)}$ could be further evaluated in terms of the jump frequency of the mth atom from an already occupied site of the sth lattice to any empty site of the s'th lattice, $w_{ss'}^{(m)}$, i.e.,

$$\omega_{ss'}^{(m)}=\left(1-\sum_{m'} p_{m's'}\right)w_{ss'}^{(m)}. \tag{7}$$

One has to note that occupancies p_{ms} are governed by the associated energy levels and the temperature within a Boltzmann statistics. Jump frequencies $w_{ss'}^{(m)}$ are governed by energy barriers between sites (including probabilities $\rho_{ss'}^{(mn)}$) and a temperature as well within the same statistics. They do depend as well on the jump frequency at ''infinite'' temperature, the latter frequency being solely dependent upon the mass of the atom, i.e., the index m. The last statements apply to a thermally driven diffusivity and a thermal equilibrium within a sample.

A diffusion matrix has dimensions $[(S\times M)\times(S\times M)]$, where S stands for the number of different lattices (number of different vortices within a chemical unit cell), while M stands for a number of different atoms constituting a crystal, i.e., $s=1,2,\ldots,S$ and $m=1,2,\ldots,M$. The simplest system, where a diffusivity could be observed under Bragg conditions, has $S=2$ and $M=1$.

A diffusion matrix is generally non-Hermitian, albeit eigenvalues are real (lesser or equal to zero). The above matrix is a correct description provided jumps expressed by the above matrix remain uncorrelated to each other. One can calculate eigenvalues and eigenvectors of the above matrix (left and right) according to the expressions

$$\hat{V}\hat{W}\hat{U}=\hat{\lambda},\ \hat{V}\hat{U}=\hat{U}\hat{V}=\hat{1},\ \det(\hat{W}-\hat{\lambda})=0, \tag{8}$$

where $\hat{V}$ stands for the matrix of left eigenvectors (eigenvectors are rows), $\hat{U}$ stands for the matrix of right eigenvectors (eigenvectors are columns), and $\hat{\lambda}$ stands for a diagonal matrix containing subsequent eigenvalues λ as diagonal elements. A symbol $\hat{1}$ denotes a unit matrix (operator).

The above eigenvalues and eigenvectors could be used in a straightforward manner to calculate the resulting scattering function $S(t)$. Namely, a scattering function under Bragg conditions follows the expressions (for an allowed Bragg reflection with nonzero intensity)

$$S(t)=\sum_{\lambda\lambda'} C_{\lambda\lambda'}\exp\{[\lambda+(\lambda')^{\star}]t\},$$

where

$$C_{\lambda\lambda'}=A_{\lambda\lambda'}\Big/\sum_{\lambda\lambda'} A_{\lambda\lambda'}$$

and

$$A_{\lambda\lambda'}=\sum_{ms}\sum_{m's'} F_{ms}(\overline{q_0}\,\overline{q\varepsilon})F^{\star}_{m's'}(\overline{q_0}\,\overline{q\varepsilon})f_{msm's'}(\overline{q})\times[p_{ms}p_{m's'}]^{1/2}\exp[i\overline{q}\cdot(\overline{r_s}-\overline{r_{s'}})]V_{\lambda'm's'}U_{ms\lambda}. \tag{9}$$

Here, $\overline{q_0}$ stands for the wave vector of the incident radiation, $\overline{q}=\overline{G}(hkl)$ stands for the wave-vector transfer to the crystal with $\overline{G}(hkl)$ being a reciprocal lattice vector having Miller indices hkl, $\overline{\varepsilon}$ stands for a unit vector perpendicular to $\overline{q_0}$ and belonging to the polarization plane of the incident radiation (note that neither stationary target nor APD detector are sensitive to the polarization of radiation—see Fig. 1 for details), and $F_{ms}(\overline{q_0}\,\overline{q\varepsilon})$ denotes a scattering amplitude of the mth atom at the sth lattice, while $f_{msm's'}(\overline{q})$ stands for the pair correlated recoilless fraction. Finally, $\overline{r_s}$ stands for the position of the sth lattice vertex within the unit cell, while $V_{\lambda'm's'}$ and $U_{ms\lambda}$ denote appropriate eigenvector elements.

Usually, one can assume that the scattering amplitude does not depend upon the lattice, and that a vibrational dynamics is uncorrelated. Hence, $f_{msm's'}(\overline{q})=[f_{ms}(\overline{q})f_{m's'}(\overline{q})]^{1/2}$, where $f_{ms}(\overline{q})$ stands for a recoilless fraction of the mth atom at the sth lattice. An assumption concerning the correlation in the vibrational dynamics is particularly well satisfied in the fast diffusivity region of temperature. A factor $A_{\lambda\lambda'}$ is invariant upon transformation $\overline{\varepsilon}\Rightarrow-\overline{\varepsilon}$ for a linearly polarized incident radiation.

One has to note that for low temperature the diffusion matrix converges to a zero matrix, and expression (9) reproduces a standard crystallographic formula describing Bragg scattering; i.e., $\Sigma_{\lambda\lambda'}A_{\lambda\lambda'}$ represents a scattering cross section from a chemical unit cell provided one chooses $\hat{V}=\hat{U}=\hat{1}$ in this temperature region. Such a representation is always possible for a zero matrix as all representations satisfying the condition $\hat{V}\hat{U}=\hat{U}\hat{V}=\hat{1}$ are admissible for that case.

IV. ANALYTICAL EXAMPLE

In order to get a better insight into the underlying physics it is worth considering some very simple example susceptible to a straightforward analytical treatment. Let us consider a monoatomic cubic crystal having a completely filled simple cubic lattice at temperature $T=0$. Let atoms occupy at higher temperatures $(\frac{1}{2}\frac{1}{2}\frac{1}{2})$ sites within a unit cell. Let the energy acquired by the atom transferred to the above site be $U_0>0$. Additionally, it is assumed that recoilless fractions and scattering amplitudes remain the same on both sites. The energy barrier for a jump from the antistructural $(\frac{1}{2}\frac{1}{2}\frac{1}{2})$ site to the structural (000) site amounts to $B>0$. A structure and corresponding barriers and energies are shown in Fig. 2. One can assume as well that transfer between sites is solely due to nearest neighbor jumps, and it could be clearly seen that all such jumps are equivalent. The probability to find an atom on the structural site is expressed as

$$p=\{1+\exp[-(U_0/T)]\}^{-1}, \tag{10}$$

and hence, it evolves from unity at $T=0$ to $\frac{1}{2}$ at ''infinite'' temperature T. The probability to find an atom on the antistructural site equals here $1-p$. Thus, a crystal approaches

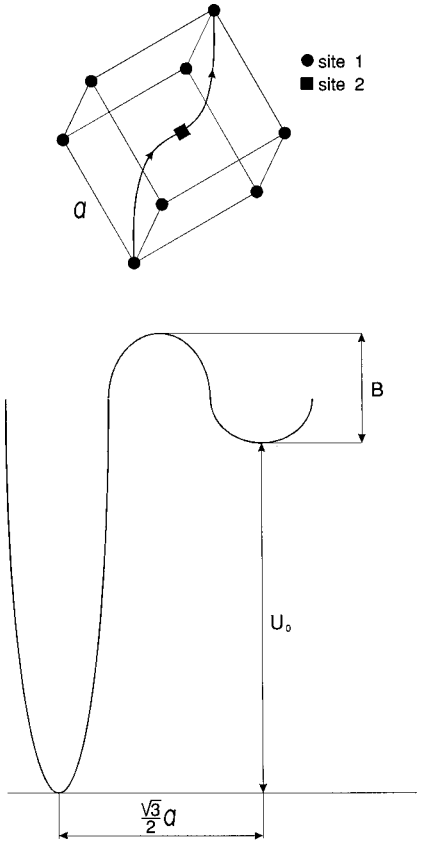

FIG. 2. Unit cell, energy levels, and barriers for the structure evaluated.

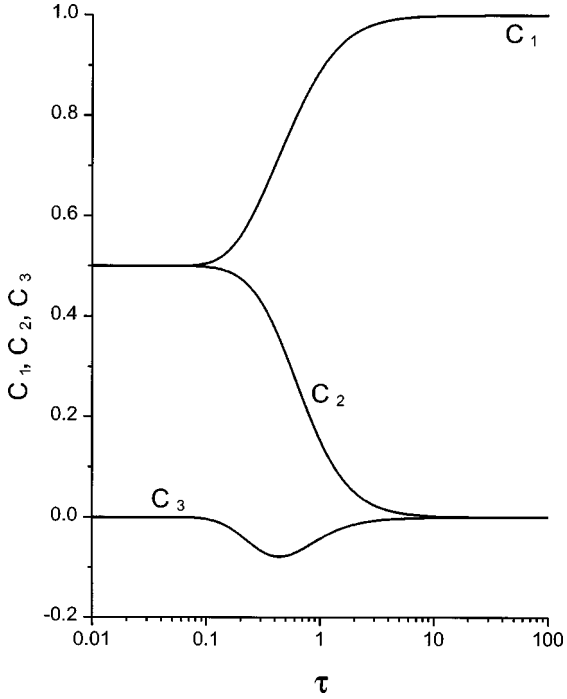

FIG. 3. Factors C_1, C_2, and C_3 plotted vs reduced temperature τ. The factors represent relative contributions from various exponents to the scattering function. For details see expression (12). The reduced temperature τ is defined as $\tau=(T/U_0)$.

at cubic (I), i.e., a body-centered structure with increasing temperature. The latter structure remains half-filled (note that for $U_0=0$ such a structure occurs at any temperature as the symmetry remains unbroken).

For a completely broken symmetry all reflections are allowed, while for the unbroken symmetry those with $h+k+l=2n+1$ are forbidden, while those with $h+k+l=2n$ are allowed. Here n stands for any integer. An effective scattering amplitude multiplied by a phase factor due to the position could be expressed for a structural site as $p^{1/2}$, while for the antistructural site as $\pm(1-p)^{1/2}$ with the $(+)$ sign referring to allowed reflections, while $(-)$ sign referring to forbidden reflections. Forbidden reflections do vanish completely at ''infinite'' temperature (or for $U_0=0$), of course. Namely, the intensity of the allowed reflection I_0 follows the expression $I_0=1+2[p(1-p)]^{1/2}$, while the intensity of the forbidden reflection I_1 obeys the relationship $I_1=1-2[p(1-p)]^{1/2}$. The latter intensities are scaled intensities, and they have to be multiplied by an atomic scattering cross section and a recoilless fraction to get measurable quantities.

Hence, a diffusion matrix takes on the following form under the assumption that jumps are uncorrelated to each other:

$$\hat{W}=-\omega\begin{pmatrix}(1-p)/p & (1-p)/p\\ 1 & 1\end{pmatrix}$$

for the forbidden reflections and

$$\hat{W}=-\omega\begin{pmatrix}(1-p)/p & (p-1)/p\\ -1 & 1\end{pmatrix}$$

for the allowed reflections, where

$$\omega=8\omega^0\left(\frac{\exp\{-[(U_0+B)/T]\}}{\{1+\exp[-(U_0/T)]\}^2}\right). \tag{11}$$

Here, ω^0 stands for a jump frequency from an occupied vertex to an empty vertex at ''infinite'' temperature. Thus, a complete model depends upon three parameters U_0, B, and ω^0 and a temperature T. One can add a lattice constant $a>0$ in order to calculate the diffusion coefficient, the latter taking the form $D=\frac{3}{8}\omega a^2$.

The above diffusion matrices describing all Bragg reflections expected have both the following eigenvalues: $\lambda_1=0$ and $\lambda_2=-(\omega/p)$. A scattering function takes on the same form for all reflections, i.e.,

$$S(t)=C_1\exp(-D_1t)+C_2\exp(-D_2t)$$

$$+C_3\exp(-D_3t),$$

where

$$D_1=0,\quad D_2=8\omega^0\left(\frac{\exp\{-[(U_0+B)/T]\}}{1+\exp[-(U_0/T)]}\right),\quad D_3=2D_2,$$

and

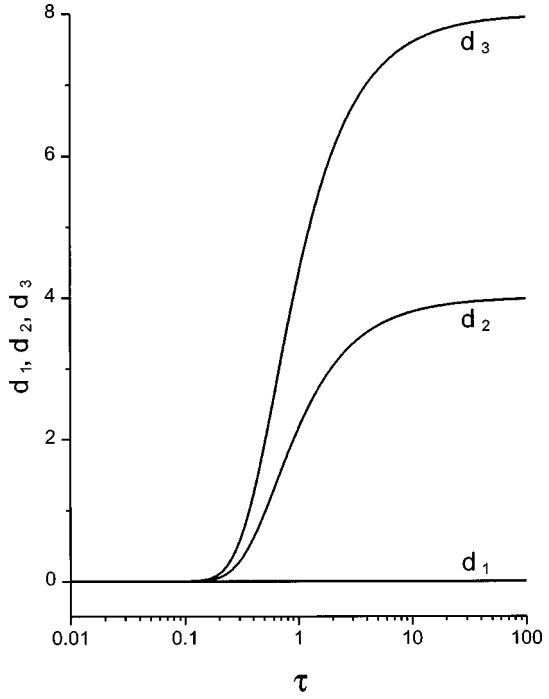

FIG. 4. Reduced decrements d_1, d_2, and d_3 plotted vs reduced temperature τ. Reduced decrements follow the expression $d_j = D_j/\{\omega^0 \exp[-(B/T)]\}$ with $j=1,2,3$ and D_j being decrements of the scattering function of expression (12).

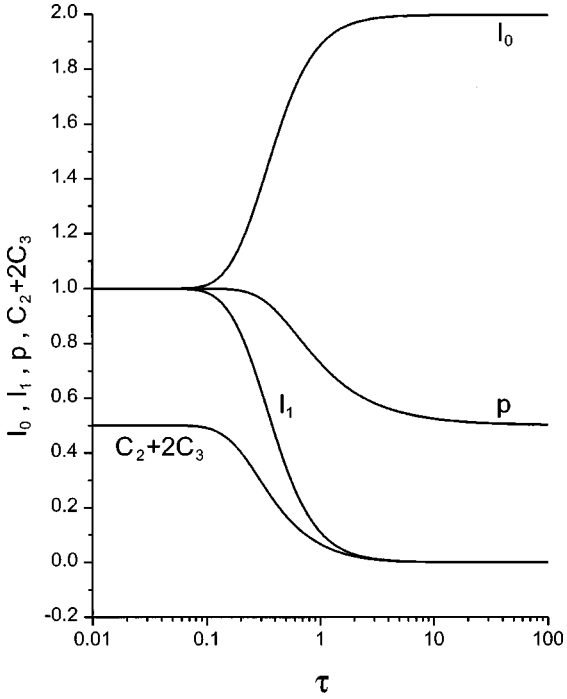

FIG. 5. Intensities I_0, I_1, probability p, and value of $C_2 + 2C_3$ plotted vs reduced temperature τ. I_0 and I_1 stand for the scaled allowed and forbidden reflections intensities, respectively, while the probability p follows expression (10).

$$C_1 = \{p^2 + [p(1-p)]^{1/2} + (1-p)^2\}/S_0,$$

$$C_2 = \{(2p-1) + (1-p)^2[(1-p)/p]^{1/2} - p[p(1-p)]^{1/2}\}/S_0,$$

$$C_3 = ([p(1-p)]^{1/2}\{2[p(1-p)]^{1/2} - 1\})/S_0,$$

where

$$S_0 = 2\{p - [p(1-p)]^{1/2}\} + [(1-p)/p]^{1/2}. \qquad (12)$$

One has to note that the diffusion matrices are non-Hermitian except at ''infinite'' temperature. Due to that, a C_3 factor takes on negative values.[20] However, an observable scattering function equals unity at $t=0$ and decays monotonically (weakly) with increasing time for all physically acceptable values of the model parameters and at any physically accessible temperature. The factors C_j $(j=1,2,3)$ are plotted versus reduced temperature $\tau=(T/U_0)$ in Fig. 3. Reduced decrements of the scattering function $d_j = D_j/\{\omega^0 \exp[-(B/T)]\}$ are shown versus τ in Fig. 4. Note that for $U_0=0$ a reduced temperature is ''infinite'' regardless of the real temperature value.

A good measure of the scattering function monotonicity versus time is the value C_2+2C_3 which has to remain non-negative at all temperatures in order to assure that $S(t)$ never grows for non-negative times.

Values of I_0, I_1, p, and C_2+2C_3 are plotted versus reduced temperature in Fig. 5. One can see that the monotonicity conditions are satisfied.

It is interesting to calculate a contribution to the heat capacity due to the above diffusive process. The latter heat capacity per atom takes on the following form under constant pressure:

$$C_p = k_B (U_0/T)^2 \times (\exp[-(U_0/T)]/\{1+\exp[-(U_0/T)]\}^2), \qquad (13)$$

where k_B stands for the Boltzmann constant. A reduced diffusion coefficient d, having the form $d = D/\{\omega^0 a^2 \exp[-(B/T)]\}$, and a reduced heat capacity C_p/k_B are plotted versus τ in Fig. 6.

A scattering function $S(t)$, calculated for the values

$$U_0 = 8000\,\mathrm{K},\ B = 7900\,\mathrm{K},$$

$$\omega^0 = 10^{13}\,\mathrm{s}^{-1},\ \text{and}\ T = 1000\,\mathrm{K},$$

is shown versus elapsed time t in Fig. 7. One has to note that for the above values of parameters and temperature, and additionally for $a=3$ Å one obtains $D = 3.36\times10^{-9}$ cm^2 s^{-1} for a diffusion coefficient.

Finally, Fig. 8 shows the expected signal $I(t)$ versus time t calculated for the above scattering function and

$$\gamma = 0.00709\,\mathrm{ns}^{-1},\ L_0 = 2,\ \text{and}\ |v| = 4.793\,\mathrm{mm/s}.$$

The parameter b has been set to zero; i.e., it has been assumed that the TDS contribution is negligible.

The above values correspond to the ^{57}Fe 14.4 keV line, where $q_0 = 7.302\,54$ Å^{-1}. It seems that for the latter line the best resonant targets are polycrystalline Rh foils having

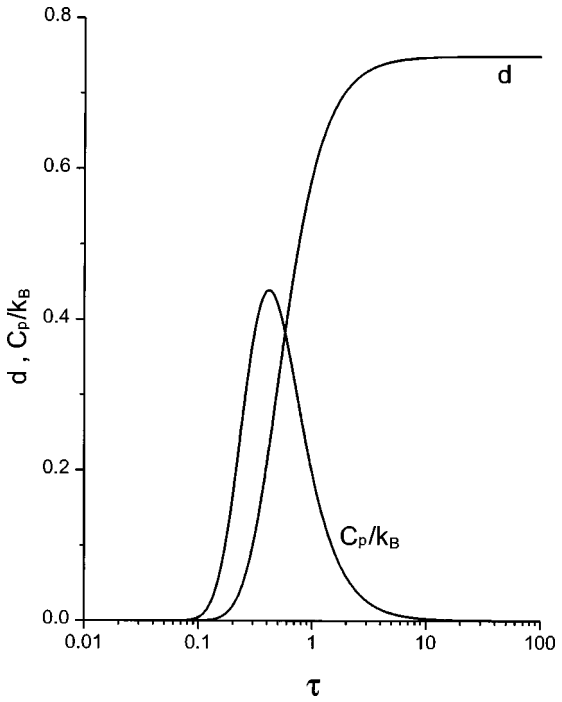

FIG. 6. Reduced diffusion coefficient d and reduced heat capacity C_p/k_B plotted vs reduced temperature τ. The reduced diffusion coefficient equals $d=D/\{\omega^0 a^2 \exp[-(B/T)]\}$ with D being a diffusion coefficient, while a heat capacity C_p is defined by expression (13).

about 6 μm thickness with several at. % of ^{57}Fe randomly alloyed in. Such targets could be kept in the vicinity of room temperature.

For a completely elastic scattering one would get here a 100% modulation depth at all times. A gradually diminishing

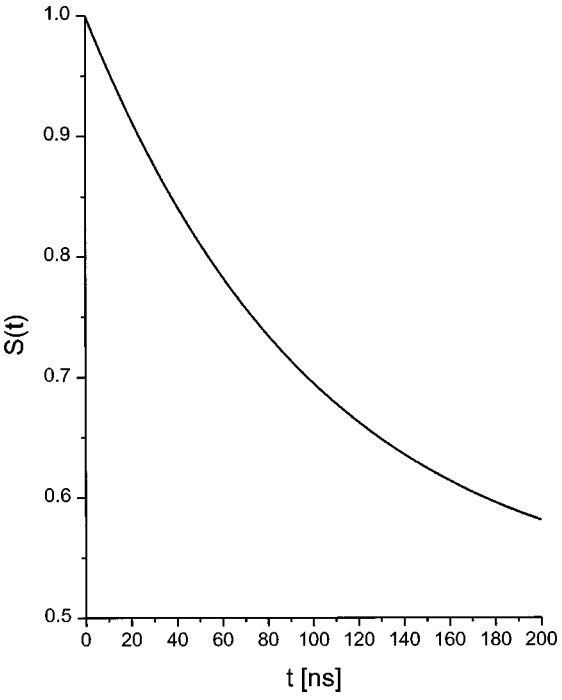

FIG. 7. Scattering function $S(t)$ plotted vs time t. The scattering function is defined by expression (12).

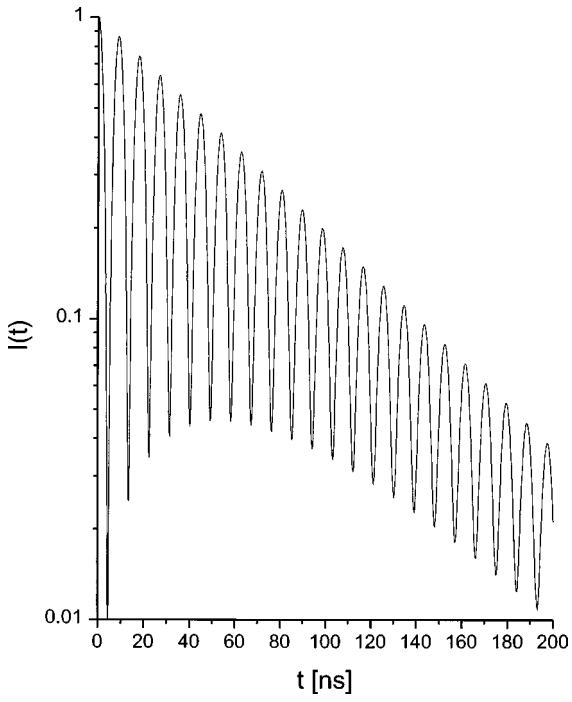

FIG. 8. Signal $I(t)$ plotted vs time t. This is a detector signal normalized to unity at the instant of prompt.

modulation depth with time elapsed is an indication of the quasielastic processes in a scattering mechanism. A curve joining the maxima of the $I(t)$ function depends on the scattering function as well, but a decrease in the modulation depth is a major effect. One has to take into account the fact that an overall time resolution of the system including the number of channels used to store the data has an influence on the modulation depth. Hence, the time resolution has to be as good as possible.

It is interesting to note that for the model outlined above one can get almost 50% of the quasielastic component in the scattered radiation, however for a strong symmetry breaking. In the case of complete symmetry one obtains a purely elastic signal in accordance with the principle that no broadening occurs under Bragg conditions for jumps within a Bravais lattice either primitive or nonprimitive.

A gradual vanishing of the quasielastic component with increasing temperature could be interpreted as well as some kind of motional narrowing.

One has to note as well that the main contribution to the quasielastic component comes from the ''interference terms,'' the latter being present solely due to the coherent character of the scattering under Bragg conditions.

A scattering function would work in a similar way in an incoherent channel (a scattering function would be generally different) as the original coherency is due rather to the instrument than the sample investigated. However, an incoherent intensity in a narrow geometry would be almost null.

A diffusion matrix for the above example converges to a zero matrix for a sufficiently low temperature; however, there is no need to switch to a diagonal representation as long as one is interested solely in the scattering function $S(t)$ as all eigenvalues converge to zero as well. The last statement is of the general character for a thermally driven diffusivity, and thus it would apply to any diffusion matrix.

V. CORRELATED JUMPS

Correlated jumps cannot be described in a standard diffusion matrix approach[18] for Bragg scattering. One has to introduce an abstract orthogonal configuration space having each dimension associated with a different configuration within a chemical unit cell. A diffusivity mechanism leads to transitions between various configurations, and hence, transition frequencies describe frequencies of the ''events''[21] leading from one to another configuration instead of simple ''elementary'' atomic jumps.

The diffusion matrix elements in configuration space take on the form

$$W_{ll'}=\Omega_{ll'}\alpha_{ll'}(\overline{q}) \text{ for } l'\neq l$$

and

$$W_{ll}=-\sum_{l'\neq l}\Omega_{ll'} \text{ for } l'=l, \tag{14}$$

where the index l enumerates distinct configurations, while the symbol $\Omega_{ll'}$ stands for a frequency of transition from the lth to the l'th configuration.

The geometrical factor $\alpha_{ll'}(\overline{q})$ becomes quite complicated for correlated jumps except for the simplest cases. Namely, it takes on the following form:

$$\alpha_{ll'}(\overline{q})=N^{-1}\sum_{m}\sum_{ss'}p_{ms}^{(l)}p_{ms'}^{(l')}\sum_{n}(l'|\rho_{ss'}^{(mn)}|l)$$

$$\times\exp(i\overline{q}\cdot[\overline{R}_{s'}^{(n)}-\overline{R}_{s}]),$$

with

$$N=\sum_{m}\sum_{ss'}p_{ms}^{(l)}p_{ms'}^{(l')}\sum_{n}(l'|\rho_{ss'}^{(mn)}|l)>0. \tag{15}$$

Here, $p_{ms}^{(l)}$ stands for a probability to find the mth atom at the sth lattice within the lth configuration, the symbol $(l'|\rho_{ss'}^{(mn)}|l)$ stands for a weight replacing weight $\rho_{ss'}^{(mn)}$, and the remaining symbols have the same meaning as in expression (3). One can again conclude that $\alpha_{l'l}(\overline{q})=[\alpha_{ll'}(\overline{q})]^{\star}$.

For a system being at equilibrium (such conditions are always satisfied for the setup under consideration) one obtains again

$$p_l\Omega_{ll'}=p_{l'}\Omega_{l'l} \text{ for } l'\neq l$$

and

$$\Omega_{ll'}=[p_lp_{l'}\omega_{ll'}\omega_{l'l}]^{1/2} \text{ for } l'<l,$$

with

$$p_l\omega_{ll'}=p_{l'}\omega_{l'l} \text{ for } l'\neq l \text{ and } \sum_{l}p_l=1, \tag{16}$$

where p_l stands for the probability to find a unit cell in the lth configuration, and $\omega_{ll'}$ denotes a scaled transition frequency due to flux (current) conservation under equilibrium. One has to note that the probabilities follow Boltzmann statistics, while the scaled frequencies are governed again by the energy levels, energy barriers, and some limiting frequencies at very high temperatures. For a very low temperature all scaled frequencies converge to zero, resulting in a zero diffusion matrix in configuration space.

The scattering function $S(t)$ follows expression (9), albeit with factors $A_{\lambda\lambda'}$ taking the form

$$A_{\lambda\lambda'}=\sum_{ll'}(p_lp_{l'})^{1/2}\Bigg[\sum_{ms}\sum_{m's'}F_{ms}^{(l)}(\overline{q_0}\overline{q\varepsilon})[F_{m's'}^{(l')}(\overline{q_0}\overline{q\varepsilon})]^{\star}$$
$$\times f_{msm's'}^{(ll')}(\overline{q})[p_{ms}^{(l)}p_{m's'}^{(l')}]^{1/2}$$
$$\times\exp[i\overline{q}\cdot(\overline{r_s}-\overline{r_{s'}})]\Bigg]V_{\lambda'l'}U_{l\lambda}. \tag{17}$$

The meaning of the symbols is obvious, while comparing the above expression with expression (9). Usually, one can assume that scattering amplitudes $F_{ms}^{(l)}(\overline{q_0}\overline{q\varepsilon})$ depend neither upon the configuration nor the lattice. The vibrational dynamics is likely to remain uncorrelated and configuration independent as well. It is important to use a complete set of all lattices in order to obtain correct results. Actually, some of them might remain empty for particular configurations.

A configuration space chosen has to have enough dimensions to assure that all configurations remain uncorrelated one to another. Hence, it might be necessary to enlarge a unit cell in some more complex cases.

The above formalism reproduces exactly the scattering function $S(t)$ evaluated in a Sec. IV for a *B2*-structure compound having the following properties: (1) both lattices are almost completely filled at all temperatures, (2) (0 0 0) sites are filled solely by $m=1$ atoms and $(\frac{1}{2}\frac{1}{2}\frac{1}{2})$ sites by $m=2$ atoms at a low temperature, and (3) the system remains at equilibrium and a diffusivity causes ''instantaneous'' inversion of random nearest neighbor atomic pairs, leading at a high temperature to a random, albeit still stoichiometric, alloy. The unit cell sketched in Fig. 2 applies to the above compound. It is additionally assumed that recoilless fractions are lattice independent.

One has to reinterpret model parameters, of course. The energy U_0 stands here for an energy of the inverted pair (for the $U_0=0$ random alloy exists at all temperatures) and B denotes a barrier for the relaxation of the inverted pair to a normal pair, while ω^0 is a limiting frequency of inversion at very high temperatures.

The probability p stands for the probability to find a normal unit cell, while C_p is a contribution to the heat capacity per unit cell. The diffusion coefficient due to the above process is the same for both atoms and it follows the same expression as outlined in Sec. IV. However, even a small concentration of vacancies might cause direct jumps within particular lattices breaking the above symmetry. The latter jumps remain invisible to the scattering function. Scaled intensities I_0 and I_1 are the same as above; however, the scaling factor takes the form

$$\{f_1^{1/2}\,\mathrm{Re}(F_1)\pm f_2^{1/2}\,\mathrm{Re}(F_2)\}^2$$
$$+\{f_1^{1/2}\,\mathrm{Im}(F_1)\pm f_2^{1/2}\,\mathrm{Im}(F_2)\}^2,$$

where the index $m=1,2$ enumerates atoms, the sign $(+)$ refers to the allowed reflections, and the sign $(-)$ to the for-

bidden reflections, while f_m and F_m stand for the appropriate recoilless fraction and scattering amplitude, respectively.

One has to note that forbidden reflections disappear always in a high-temperature limit for the above compound. If both kinds of atoms are the same, one restores symmetry at any temperature, and the scattering function becomes purely elastic with vanishing forbidden reflections.

Hence, a *B2*-structure compound provides another example of symmetry breaking within a nonprimitive Bravais lattice as in a high-temperature limit it represents a cubic (I) lattice with a 50% chance to find an atom of the mth kind at any vertex.

It is interesting to note that the scattering function for the last case does not depend upon the difference in ability to scatter by different atoms at different sites (except for a difference in the intensity of allowed and forbidden reflections), but it depends upon the symmetry breaking due to nonvanishing U_0 energy. The last phenomenon is caused by some kind of ''phase locking'' in the coherent process occurring here.

A small amount of vacancies would not change the conclusions reached above; albeit, it is likely to speed up diffusivity significantly.

VI. CONCLUSIONS

It has been shown that the NRSR interferometer described in Ref. 11 could be used to study relatively slow diffusive motions of atoms in single crystals in a way being sensitive to both energy and momentum transfer.

The above device performs like a selector, allowing one to see solely jumps between various Bravais lattices. Nonprimitive lattices require some symmetry breaking, leading to distinct primitive lattices in order to see jumps within them.

The range of elements susceptible to this method is quite wide, excluding the lightest elements exhibiting very small cross sections for the Rayleigh scattering dominating here. One could say that all elements accessible to the x-ray diffraction could be studied here as well. One has to avoid resonant atoms in the sample investigated.

Due to the small cross section of the beam, quite small samples could be investigated (plates having $5\times5\times0.1$ mm^3 dimensions are quite satisfactory). For such samples it is easy to maintain a homogeneous and constant temperature over the sample volume.

It might occur that this method would become as standard as x-ray diffraction, however with an extra dimension (time-energy) added.

One has to note as well that the method described above is the most precise and the fastest way to obtain a single-phonon TDS contribution under Bragg reflections. A competing method of the Rayleigh scattering of Mössbauer radiation from radioactive sources requires extremely long measurement time periods due to the very small photon flux reaching a detector[22] at a comparable energy resolution.

A configuration space approach might appear to be very useful in the case of correlated jumps as it has naturally built in a coherent behavior of the Bragg scattering.

A crystal satisfying conditions described in a Sec. IV is somewhat artificial, and it was used to illustrate principles in the simplest way. On the other hand, *B2*-structure compounds being close to the one described in Sec. V and otherwise suitable for an experimental setup outlined are quite common.

ACKNOWLEDGMENT

Dr. Bogdan Sepioł from Institut für Materialphysik der Universität Wien, Austria is warmly thanked for many inspiring discussions and constant interest in this work.

*Author to whom all correspondence should be addressed: Electronic address: sfrueben@cyf-kr.edu.pl

[1] H. Franz, A. Q. R. Baron, A. Meyer, A. I. Chumakov, R. Rüffer, W. Petry, and G. Smirnov, Jahresbericht des Instituts für Festkörperphysik E13, TU, München, 1996, p. 39.

[2] W. B. Yelon, G. Schupp, M. L. Crow, C. Holmes, and J. G. Mullen, Nucl. Instrum. Methods Phys. Res. B **14**, 341 (1986).

[3] O. G. Randl and M. R. Johnson, Neutron News **8** (4), 11 (1997).

[4] N. M. Butt and D. A. O'Connor, Proc. Phys. Soc. London **90**, 274 (1967).

[5] M. Elwenspoek, M. Soltwisch, and D. Quitmann, Mol. Phys. **35**, 1221 (1978).

[6] *Guide to Neutron Research Facilities*, edited by H. Blank and B. Maier (ILL, Grenoble, 1988), p. 62.

[7] G. Vogl, in *Mössbauer Spectroscopy Applied to Magnetism and Materials Science*, edited by G. J. Long and F. Grandjean (Plenum, New York, 1996), Vol. 2, p. 85.

[8] E. Gerdau, R. Rüffer, H. Winkler, W. Tolksdorf, C. P. Klages, and J. P. Hannon, Phys. Rev. Lett. **54**, 835 (1985).

[9] B. Sepioł, A. Meyer, G. Vogl, R. Rüffer, A. I. Chumakov, and A. Q. R. Baron, Phys. Rev. Lett. **76**, 3220 (1996).

[10] G. Smirnov, Hyperfine Interact. **97/98**, 551 (1996).

[11] A. Q. R. Baron, H. Franz, A. Meyer, R. Rüffer, A. I. Chumakov, E. Burkel, and W. Petry, Phys. Rev. Lett. **79**, 2823 (1997).

[12] K. Ruebenbauer, J. G. Mullen, G. U. Niehnaus, and G. Schupp, Phys. Rev. B **49**, 15 607 (1994).

[13] G. U. Nienhaus, H. Frauenfelder, and F. Parak, Phys. Rev. B **43**, 3345 (1991).

[14] G. Schupp, W. B. Yelon, J. G. Mullen, and R. Wagoner, Hyperfine Interact. **93**, 1491 (1994).

[15] G. Schupp, K. Barnes, W. B. Yelon, and J. G. Mullen, Hyperfine Interact. **92**, 1149 (1994).

[16] Yu. Kagan, A. M. Afanas'ev, and V. G. Kohn, J. Phys. C **12**, 615 (1979).

[17] M. Kwater, K. Ruebenbauer, and U. D. Wdowik, Physica B **190**, 199 (1993).

[18] R. Kutner and I. Sosnowska, J. Phys. Chem. Solids **38**, 741 (1977).

[19] K. Ruebenbauer, U. D. Wdowik, and M. Kwater, Phys. Rev. B **54**, 4006 (1996).

[20] K. Ruebenbauer, U. D. Wdowik, M. Kwater, and J. T. Kowalik, Phys. Rev. B **54**, 12 880 (1996).

[21] K. Ruebenbauer, B. Sepioł, and B. Miczko, Physica B **168**, 80 (1991).

[22] G. Albanese, C. Ghezzi, A. Merlini, and S. Pace, Phys. Rev. B **5**, 1746 (1972).